


NARRATIVE REVIEW



Imaging the acute respiratory distress syndrome: past, present and future

Laurent Bitker^{1,2,3*} , Daniel Talmor^{4,5} and Jean-Christophe Richard^{1,2,3}

© 2022 Springer-Verlag GmbH Germany, part of Springer Nature

Abstract

In patients with the acute respiratory distress syndrome (ARDS), lung imaging is a fundamental tool in the study of the morphological and mechanistic features of the lungs. Chest computed tomography studies led to major advances in the understanding of ARDS physiology. They allowed the *in vivo* study of the syndrome's lung features in relation with its impact on respiratory physiology and physiology, but also explored the lungs' response to mechanical ventilation, be it alveolar recruitment or ventilator-induced lung injuries. Coupled with positron emission tomography, morphological findings were put in relation with ventilation, perfusion or acute lung inflammation. Lung imaging has always been central in the care of patients with ARDS, with modern point-of-care tools such as electrical impedance tomography or lung ultrasounds guiding clinical reasoning beyond macro-respiratory mechanics. Finally, artificial intelligence and machine learning now assist imaging post-processing software, which allows real-time analysis of quantitative parameters that describe the syndrome's complexity. This narrative review aims to draw a didactic and comprehensive picture of how modern imaging techniques improved our understanding of the syndrome, and have the potential to help the clinician guide ventilatory treatment and refine patient prognostication.

Keywords: Acute respiratory distress syndrome, Ventilator-induced lung injuries, Computed tomography, Electrical impedance tomography, Positron emission tomography, Lung ultrasounds

Introduction

Lung imaging is a fundamental tool in the study of the morphological and mechanistic features of the acute respiratory distress syndrome (ARDS), and may help guide clinical management. The lungs are large organs with great morphologic heterogeneity, as they have the unique characteristic of containing, tissue, extracellular matrices, gas and a large blood compartment, requiring the use of 3-dimension imaging tools. This is supported by the variety of the lungs' response to ventilatory settings in terms

of aeration, ventilation, and perfusion. Lung imaging also offers the opportunity of studying ARDS mechanisms at a quasi-cellular level, while usual 2-dimensional imaging techniques may oversimplify lung biomechanics. From chest X-ray radiographs to quantitative computed tomography (CT), the description of ARDS morphological and mechanistic features has never been this advanced. Positron emission tomography (PET), with its high specificity and sensitivity for biochemical processes, has led to major advances in our understanding of the pathogenesis of ARDS and of ventilator-induced lung injuries (VILI). Using lung ultrasounds (LUS) or electrical impedance tomography (EIT), the clinician can personalize mechanical ventilation at the bedside.

This review aims to draw a comprehensive picture of how medical imaging improved our understanding of the syndrome, and how different imaging modalities further improve our knowledge and enhance personalized care of ICU patients with ARDS.

*Correspondence: laurent.bitker@chu-lyon.fr

¹ Service de Médecine Intensive – Réanimation, Hôpital de la Croix Rousse, Hospices Civils de Lyon, 103 Grande Rue de la Croix Rousse, 69317 Lyon Cedex 04, France

Full author information is available at the end of the article

Imaging and physiopathology

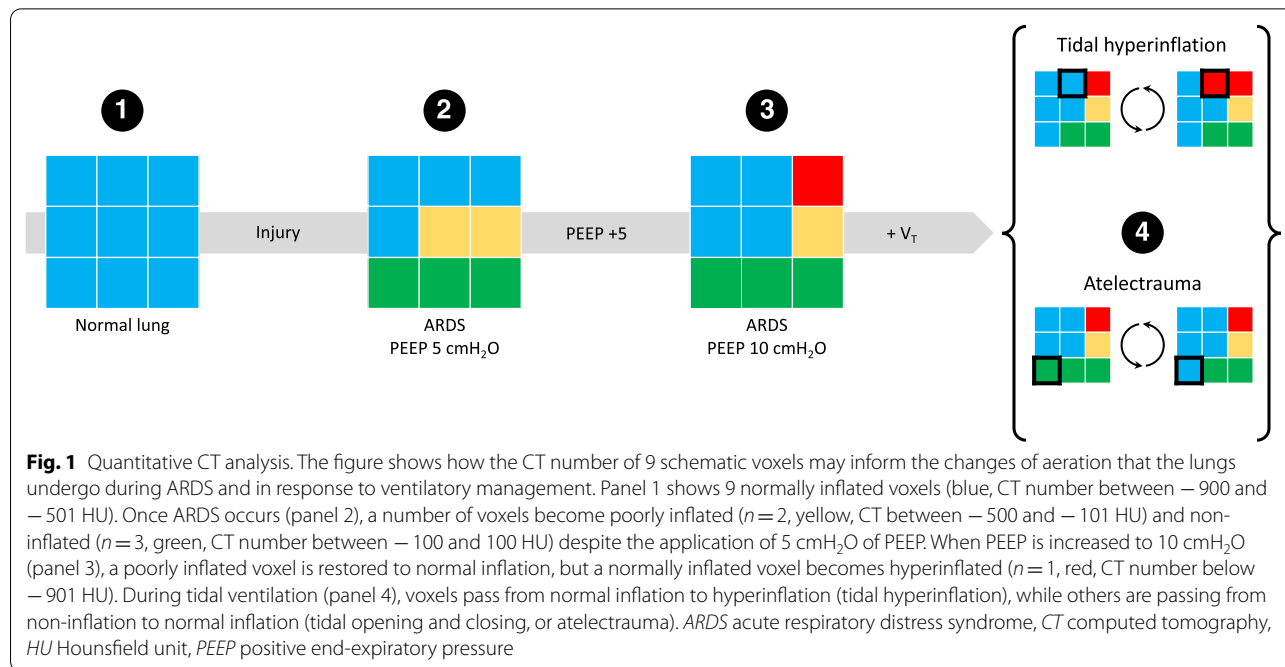
Since the description of ARDS in 1967, lung imaging has been a key element of the syndrome's definition and all ARDS definitions have included imaging criteria [1]. ARDS can present with morphological features such as alveolar consolidation, ground-glass opacities, interstitial edema with reticular patterns, or normally appearing lung parenchyma. However, none of these elements are specific to ARDS [2]. These radiologic findings, which are preferentially located in dependent regions, are the consequences of alveolar flooding by edema, inflammatory interstitial edema, and congestion of pulmonary capillaries. Consequently, chest X-ray radiography remains essential to the initial diagnosis of ARDS as a first-line imaging tool, and is useful for daily clinical management [3].

Take-home message

The complexity of the lung injury in acute respiratory distress syndrome (ARDS) compels the use of 3-dimensional imaging tools, such as computed tomography, lung ultrasounds, electrical impedance tomography or positron emission tomography, capable of capturing heterogeneity from apex to lung base, and accounting for the spatial distribution of aeration, ventilation and perfusion. Lung imaging, be it in the experimental setting, or at the bedside of critically ill patients with ARDS, has led to major advances in the understanding and management of the syndrome, and has the potential to guide ventilatory and non-ventilatory strategies in the near future

Quantitative CT imaging

The variety and extent of CT findings, such as dependent alveolar consolidation or diffuse ground-glass opacities, allowed their extensive study and correlation with the



(See figure on next page.)

Fig. 2 Representative lung CTs before and after ARDS induction in swine. The upper part of the figure shows 2 CT slice at mid-chest level in the same animal under mechanical ventilation, general anesthesia and neuromuscular blockade. CTs are acquired at end-expiration, before and after experimental ARDS is induced by intratracheal instillation of hydrochloric acid. The CT image on the right shows typical ARDS CT findings, with dependent alveolar consolidation and ground-glass opacities in the mid-level section. The medial part of the figure shows the distribution of CT numbers of the CT slices presented above, after the exclusion of extra-pulmonary areas by manual segmentation. To better represent the change in inflation, CT numbers were classified based on 4 inflation compartments: non-inflated (CT number between -100 and 100 HU), poorly inflated (CT number between -500 and -101 HU), normally inflated (CT number between -900 and -501 HU) and hyperinflated (CT number below -900 HU). The histograms clearly demonstrated how the non-aerated compartment increases, and the normally inflated compartment is diminished as a consequence of experimental ARDS. Finally, the lower part of the figure shows the parametric images of inhomogeneities based on the patented method by Cressoni and colleagues in the same CT slices (patent WO 2013/088336A1 "Method for determining inhomogeneity in animal tissue and equipment to implement it"). The image on the right shows how ARDS increases lung inhomogeneities, especially in zones at the interface of regions with different aeration (voxels in red). ARDS acute respiratory distress syndrome, CT computed tomography, HU Hounsfield unit

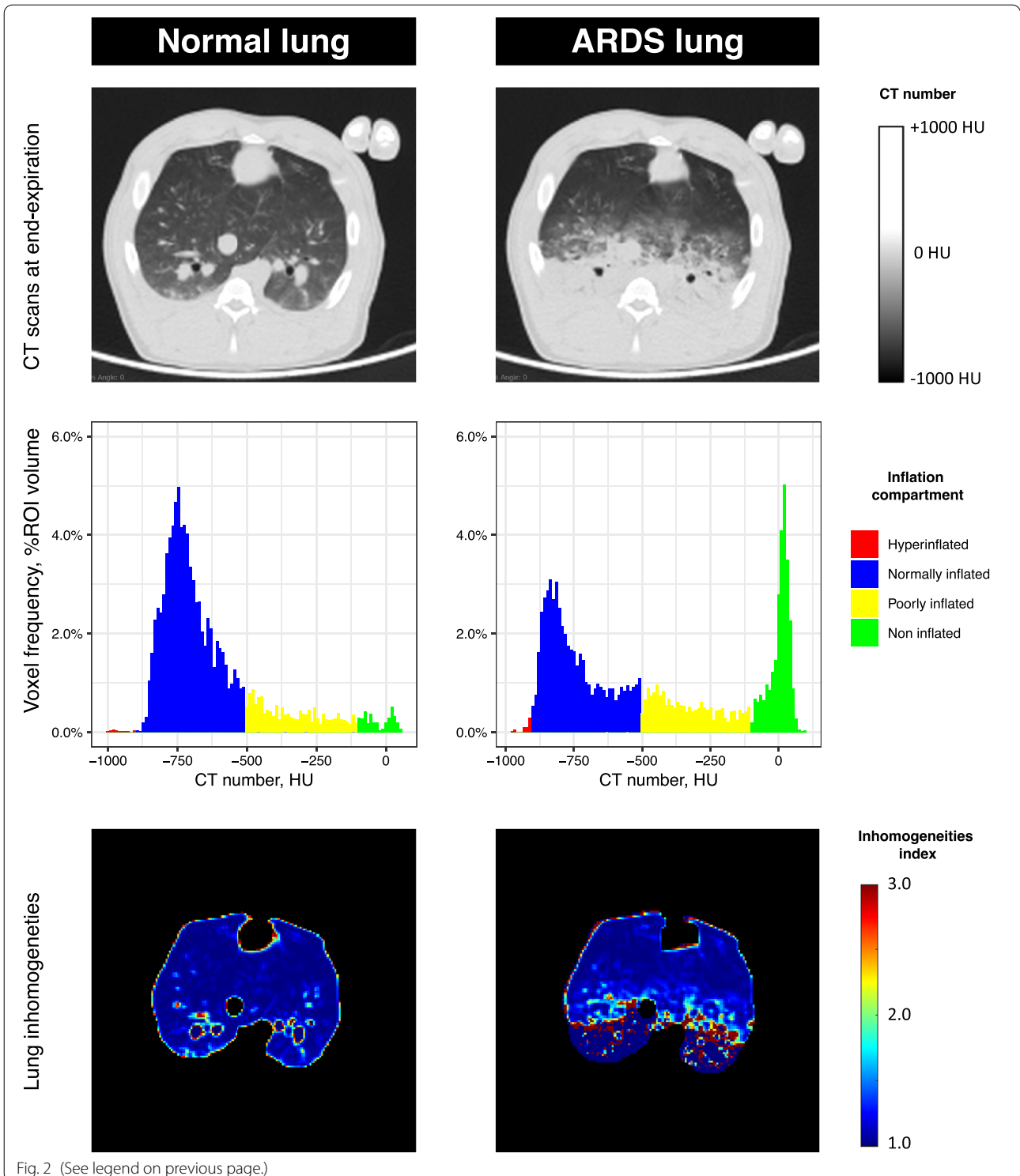


Fig. 2 (See legend on previous page.)

physiological shunt, degree of hypoxia, and clinical history of the disease [4–6]. With the increase in computing power, came the era of quantitative CT, which led to further description of the syndrome’s characteristics, in

terms of quantification of the loss in the aerated compartment (the baby lung) or the non-invasive quantification of the lungs’ extra-weight (as a marker of the edematous injury) and non-aerated compartment extent, as well as

the description of the effects of positive end-expiratory pressure (PEEP) and tidal volume (V_T) on lung recruitment, inflation and hyperinflation (Fig. 1) [4, 7–9]. Using the voxels' CT number, in Hounsfield units (HU), one can also classify the lung as being non-aerated, poorly-aerated, normally-aerated, or hyperinflated, and follow the evolution over time of these four clusters [10]. An important finding is that the distribution of CT numbers are dramatically shifted towards 0 (the CT number of water) in ARDS (Fig. 2) [4].

By performing coupled CT image acquisitions at end-expiration and end-inspiration in ventilated patients without spontaneous breathing, differences in aerated volumes correspond to the CT-derived regional V_T (Fig. 1). This allowed the study of the correlation of CT parameters with respiratory mechanics, and helped describe how the decrease in aerated volume led to high lung elastance, rather than the intrinsic change in specific lung elastance [11]. Furthermore, repeated CT scans in dogs with oleic acid-induced ARDS exposed to increasing airway pressures allowed the identification of the pressure at which the lung “reopens”, demonstrating that ARDS lungs may be recruited albeit at the price of excessively high intra-thoracic pressures [12].

More recently, the heterogeneity of lung abnormalities was quantified using a method developed by Cresoni and colleagues. By comparing the inflation of a given voxel to that of its surrounding voxels, the authors produced parametric maps of the heterogeneity of aeration using a single CT acquisition, estimating the regional stress raisers at the interface of regions with different compliance (Fig. 2) [13]. This parameter was shown to increase over time in pigs ventilated with injurious settings, and its extent above a certain species-specific threshold was associated with worse individual outcome [13, 14].

Regional perfusion and ventilation

PET functional lung imaging has allowed further description of ventilation and perfusion alterations that occur in ARDS. Vidal Melo and colleagues showed that ARDS was characterized by a considerable perfusion-ventilation mismatch in mechanically ventilated sheep, with ventilation directed to anterior, non-perfused regions, and perfusion mainly distributed to dorsal, non-aerated regions [15]. However, this redistribution is variable across subjects, and may explain why individuals with similar ARDS severity in CT may have very different $\text{PaO}_2/\text{FiO}_2$ ratios [16]. This perfusion-ventilation mismatch may be amplified by inappropriate PEEP levels, which may preferentially direct blood flow to dependent non-aerated regions (see below) [17].

More recently, EIT allowed the study at the patient's bedside of regional ventilation, using changes in lung tissue impedance to detect relative changes in inflation and aeration induced by modification of ventilatory settings [18]. Although this technique is limited in its spatial resolution and field of view, its strength relies on its temporal resolution, allowing the detection of dynamic phenomena occurring during lung inflation or deflation. Richard and colleagues showed that EIT and PET measurements of regional ventilation were well correlated and within narrow limits of agreements in swine with acute lung injury [19].

Lung imaging and clinical management PEEP and alveolar recruitment with CT

The effect of PEEP on regional lung aeration was first described by Gattinoni and colleagues, in relation to an improvement in oxygenation and shunt fraction when alveolar recruitment occurred [8, 13]. They observed that lung recruitment by PEEP was extremely heterogeneous and difficult to predict using respiratory mechanics and gas exchange in a large cohort of ARDS patients [20]. They also observed that lung recruitment increased with the extent of the non-aerated compartment at PEEP 5 cmH_2O , and was larger in the most severe cases of ARDS [20]. As a consequence, higher PEEP levels were also shown to induce dorsal redistribution of V_T [9]. Yet, the opening pressure required to perform a fully “open lung” strategy to prevent atelectrauma and decrease lung inhomogeneities were well above 15 cmH_2O and thus may not be compatible with the prevention of volutrauma if it exceeds the inspiratory capacity in combination with conventional V_T [21–23]. Of note, in this study, a PEEP increase from 5 cmH_2O to 15 cmH_2O was responsible for 50% of the recruitment achieved at PEEP 45 cmH_2O indicating that a compromise may be needed between recruitment and hemodynamic impairment. CT studies identified that the response to PEEP in terms of alveolar recruitment may lead to overdistension of normally aerated regions [24]. Overdistension can subsequently induce the redirection of blood flow to dependent non-aerated regions due to the PEEP-induced compression of anterior peri-alveolar capillaries, which would hamper or even reverse the expected response to PEEP on hypoxemia [17]. Some authors recently suggested the use of recruitment to hyperinflation ratio to choose the best trade-off when setting PEEP and V_T in patients with ARDS [25].

While quantitative assessment has remained to date a research tool, the visual assessment of alveolar recruitment on 2 CTs acquired at 2 PEEP levels has recently been shown to be robust enough to allow quantification

of the recruitment potential as a readily available technique in the usual care [26]. In more pragmatic terms, the use of CT protocols to assess the lungs' response to PEEP has clearly demonstrated their usefulness, but remains limited in clinical use due to difficulties to transport patients to the imaging facility and the lack of undisputable proof of an impact on patient prognosis.

PEEP and alveolar recruitment with LUS

At the bedside, LUS may be a useful tool to guide the clinician to choose the best PEEP. Using a systematic LUS protocol exploring 12 lung regions, Bouhemad and colleagues demonstrated a good correlation between lung recruitment identified on the pressure–volume curve, and the ultrasound reaeration score [27]. A major limitation of this study was that no gold standard of lung recruitment was used to confirm these results. Using a simplified protocol, exploring only posterior dependent regions, others have shown a decrease in the non-aerated area measured in LUS imaging with increasing PEEP levels, in relation to improved oxygenation [28]. Because the LUS-based methods do not quantify hyperinflation, it must be notified that using exclusively these methods may drive the clinician towards selecting higher PEEP, as

the downside effects of PEEP (hyperinflation, hemodynamic impairment) are neglected [29].

PEEP and alveolar recruitment with EIT

Point-of-care EIT has the advantage of allowing continuous bedside evaluation of the patients' ventilation pattern. It allows the monitoring of regional end-expiratory impedance in response to varying PEEP levels, with a good correlation with changes in end-expiratory lung volumes [30]. Also, EIT identifies lung recruitment if a region is deemed "silent" at a low PEEP level (i.e., the regional change in impedance, ΔZ , is null as it is not aerated, and hence non-ventilated), and regional ventilation appears at a higher PEEP level (with a detectable ΔZ due to re-aeration and resuming of regional ventilation) [31, 32].

Furthermore, using the regional variations of ΔZ induced by changes in PEEP, multiple indices of lung recruitment have been proposed, such as the ventilation map that shows how ΔZ is distributed along the antero-posterior axis, or the left-to-right direction [33]. Hence, ventilatory strategies can quantify how the relative distribution of ventilation is homogenized between anterior and posterior segments. EIT also allows the estimation of regional lung compliance, by dividing the voxel ΔZ by the

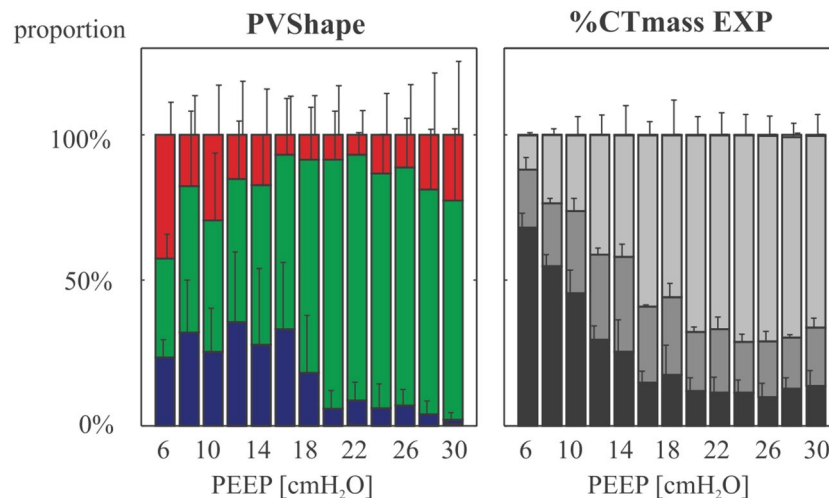


Fig. 3 Inflation response to PEEP evaluated in lung EIT and quantitative CT in patients with ARDS. The figure shows the average proportion of the 3 inflation compartments derived from the innovative methods proposed by Beda and colleagues in which EIT ΔZ , as a surrogate of volume, is used to compute a pressure–volume response curve at each PEEP level of a decremental PEEP ramp. Red bars are the proportion of voxels estimated to be exposed to tidal hyperinflation, blue bars those that undergo tidal collapse, and green bars voxels in which the change in the P–V curve is linear and ventilation is considered homogenous. These EIT-derived parameters are compared to CT-derived inflation compartments at end-expiration and at the same PEEP levels (on the right side). Inflation compartments in CT are defined as follows: non-aerated (–100 to 100 HU, black bars), poorly aerated (–500 to –101 HU, dark grey bars), normally aerated (–900 to 501 HU, light grey bars), and hyperaerated (–1000 to –901 HU, white bars). The authors conclude that there was a significant correlation between the EIT-computed overdistension parameter and non-inflated volumes at low PEEP levels, and with hyperinflated volumes at high PEEP levels, although the strength of correlation were weak. CT computed tomography, EIT electrical impedance tomography, PEEP positive end-expiratory pressure. Reproduced with permission from Wolters Kluwer Health [42]

respiratory system driving pressure. When performing a decrementing PEEP ramp, one can identify significant collapse or overdistention, when the ΔZ -based compliance decreases below, or above the best-compliance PEEP level, respectively (Fig. 3). This may guide PEEP choice, by selecting the one PEEP that offers the best compromise between collapse and overdistention, with the downside that this empirically assumes that both phenomena are equally deleterious.

Using a three-step process aiming to maximize recruitment and minimize PEEP-related overdistention in a swine ARDS model, Wolf and colleagues showed that their strategy significantly led to the use of increased PEEP levels, improved lung compliance and oxygenation [33]. Using a more complex algorithm, Becher and colleagues used EIT to set both PEEP and V_T in 20 patients with ARDS, and showed that this strategy also led to higher PEEP levels, while only limitedly affecting V_T settings, and induced significant increases in mechanical stress and strain on the one (negative) hand, and $\text{PaO}_2/\text{FiO}_2$ ratios on the other [34]. A similar strategy was evaluated in 15 humans with ARDS under extracorporeal membrane oxygenation (ECMO); the authors showed that the best PEEP based on their algorithm was between 5 and 15 cmH_2O , and could lead to a 30% extent of overdistended zones while reducing alveolar collapse to 0% at PEEP 15 cmH_2O [35]. Conversely, this study showed that the best PEEP was 5 cmH_2O in a third of enrolled severe ARDS patients treated with ECMO. Finally, in a large randomized, open label, controlled trial comparing an EIT-based PEEP selection versus a low PEEP- FiO_2 table, the authors concluded in no difference in PEEP levels, oxygenation, and clinical outcome [36]. Taken together, these results clearly demonstrate that the priority is PEEP individualization in these patients.

Tidal inflation and tidal hyperinflation in CT

The deleterious consequences of inappropriate V_T settings on the lung parenchyma have been known for decades. Excessive V_T rapidly leads to ventilator-induced lung injuries in experimental models, that can be witnessed by the appearance of lung consolidation with increased lung weight, and barotrauma [37]. Second, V_T toxicity is directly related to the remaining aerated volume, namely the “Baby Lung”; this relationship between V_T and end-expiratory lung volume (EELV) is named dynamic strain [38]. Regional dynamic strain may be quantified regionally or at voxel level with CT (using 3D deformation tools), and is associated with increased lung inflammation in experimental models of VILI [39, 40].

When tidal inflation leads to tidal hyperinflation (change in hyperinflated volume between end-expiration and end-inspiration), patients presented with a higher

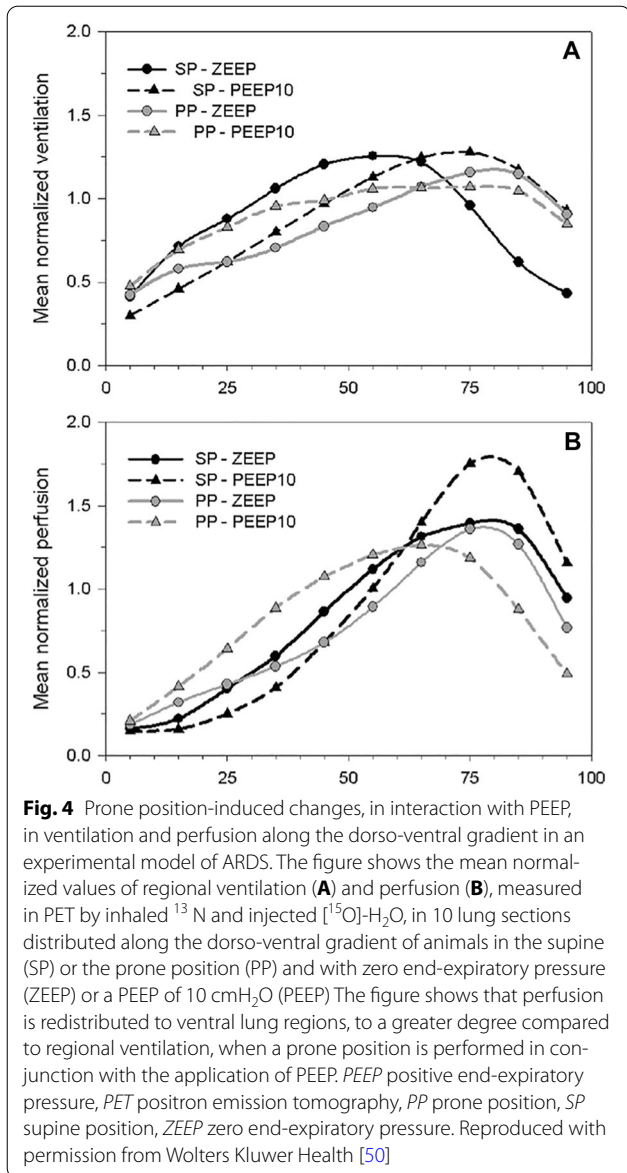
risk of mortality, even though their plateau pressure remained controlled [10]. Hyperinflation (or hyperaeration) is a marker of excessive V_T , and must be distinguished from overdistention which relates to excessive alveolar stress. The amount of tidal hyperinflation is not only related to V_T setting but also directly to the applied PEEP, which increases the EELV and shifts aeration compartments towards lower CT values. Other methodological pitfalls regarding tidal hyperinflation are the significant impact of CT reconstruction kernels on hyperinflated CT compartments, and the unknown significance of the widely used threshold of -900 HU to define it [41].

Tidal inflation and tidal overdistension with EIT

In addition to optimizing recruitment as described above, EIT may also help clinicians quantify regional ventilation and tidal overdistension at the bedside. EIT has received increasing interest due to its ability to detect intratidal regional overdistension. Beda and colleagues identified overdistension using the shape of the pressure–volume curve and dynamic EIT acquisitions suggesting that EIT has the potential to detect excessive V_T at the regional level and could help personalization of V_T [42, 43]. Another feature of EIT is that it can study intratidal events such as the pendelluft phenomenon. This term, which describes the transition of gas from one lung region to another, is frequently due to diaphragmatic efforts which redirect gas to dependent and caudal regions, by generating the collapse of anterior and cephalic regions [44]. Hence, Muders and colleagues identified that regional ventilation was delayed in certain lung regions during experimental acute lung injury, and showed that it correlated to tidal recruitment [45].

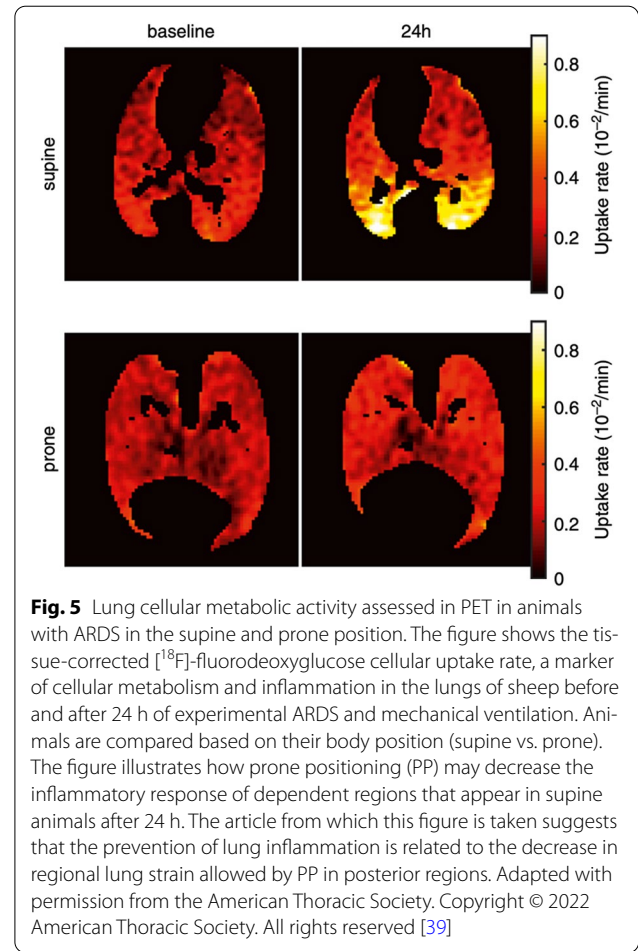
Imaging the effects of prone position on ventilation and perfusion

Gattinoni and colleagues first performed in 1991 chest CT acquisitions of patients with ARDS in the prone (PP) and the supine position (SP). They showed that the amount of edema measured in CT was unaffected by the body position, but that aeration was redistributed to the posterior regions of patients in PP. They hence coined the concept of a sponge-like lung, which acts as a viscoelastic body in which the excess weight of superior lung sections compresses inferior levels [46]. When coupled with PEEP trials, PP enhances lung recruitment potential quantified in CT, while decreasing tidal hyperinflation and atelectrauma, a finding directly related to the homogenization of aeration and ventilation induced by the body position [47]. Perchiazzi also observed that CT-estimated lung strain was mainly distributed to dependent lung regions in animals in SP without experimental ARDS and



that PP led to radical homogenization of strain between dependent and non-dependent regions, compared to SP [48].

The impact of PP on shunt fraction and hypoxemia was explained by the combined evaluation of ventilation and perfusion with PET [49]. Prone position, while recruiting dorsal regions, increases their ventilation, while perfusion remains predominant in these regions whatever the position, improving ventilation-perfusion matching at low PEEP. At higher PEEP, ventilation and perfusion are driven toward ventral regions (as a possible consequence of overdistension) (Fig. 4) [50, 51]. In parallel, the shunt fraction decreased in the posterior regions during PP [52].



Imaging lung inflammation

The non-invasive quantification of lung inflammation has remained one of the great challenges of modern ARDS imaging. The principal radiotracer used in experimental and clinical studies was fluorodeoxyglucose (^{18}F) ($[^{18}\text{F}]\text{-FDG}$), which quantifies the cellular glucose-specific metabolic demand. Its principal advantages are its widespread availability, as well as the existence of advanced quantification methodology using kinetic models developed specifically for the injured lungs [53]. It is however criticized for not being specific to the inflammatory response, as some non-inflammatory cells such as pneumocytes-2 may contribute to the tracer's uptake in ARDS [54].

One of the most ground-breaking findings that was made possible by lung PET scans in humans was the description of an increased metabolic activity with $[^{18}\text{F}]\text{-FDG}$ in the anterior, apparently uninjured, lung regions of patients with ARDS [55], suggesting that a biological response could be present in normally appearing lung regions on CT. Subsequently, Musch and colleagues

showed that high volume ventilation with extreme plateau pressures increased [^{18}F]-FDG lung uptake in healthy sheep [56]. This correlation of injurious ventilation with [^{18}F]-FDG uptake was later confirmed experimentally by Retamal and colleagues who observed its correlation with lung strain at the voxel level [57]. Further answers regarding the mechanical determinants of ventilator-induced increased lung metabolic demand were given by Guldner and colleagues who demonstrated that high regional ventilation did trigger an augmentation in [^{18}F]-FDG uptake, while ventilatory settings generating tidal alveolar opening-closing were not [58, 59]. Motta-Ribeiro and colleagues demonstrated that the homogenization of aeration and lung recruitment that is induced by PP leads to lower strain quantified at voxel level in CT, compared to SP, and was associated with a non-significant decrease in [^{18}F]-FDG uptake (Fig. 5). This is the only in vivo experimental evidence that PP may decrease lung biotrauma, in direct association with its effects on lung mechanics.

Other tracers were developed to describe acute lung inflammation, aiming to overcome the limitations of [^{18}F]-FDG. *N*-benzyl-*N*-methyl-2-[7,8-dihydro-7-(2-[^{18}F] fluoroethyl)-8-oxo-2-phenyl-9H-purin-9-yl]acetamide (^{18}F -FEDAC) and 1-(2-chlorophenyl)-*N*-methyl-*N*-(1-methylpropyl)-3-isoquinolinecarboxamide (^{11}C)(R)-PK11195) PET tracers targeting the translocator protein (18 kDa) (TSPO), a receptor located on the surface of macrophages' mitochondria, were well correlated with the presence of macrophages and neutrophils within the lungs of animals with experimental ARDS [60]. [^{11}C](R)-PK11195 PET uptake was also significantly increased after 4 h of high V_T ventilation, in relation to high dynamic strain and tidal hyperinflation (Fig. 6) [40].

The main limitation of PET imaging of lung inflammation is that the high tissue heterogeneity, due to the co-presence of air, tissue and blood, is well below the spatial resolution of this technique. Multiple efforts have been made to correct this [61, 62]. Other limits of the translatability of PET lung imaging to the clinical setting include PET camera availability, PET radiotracer production, and

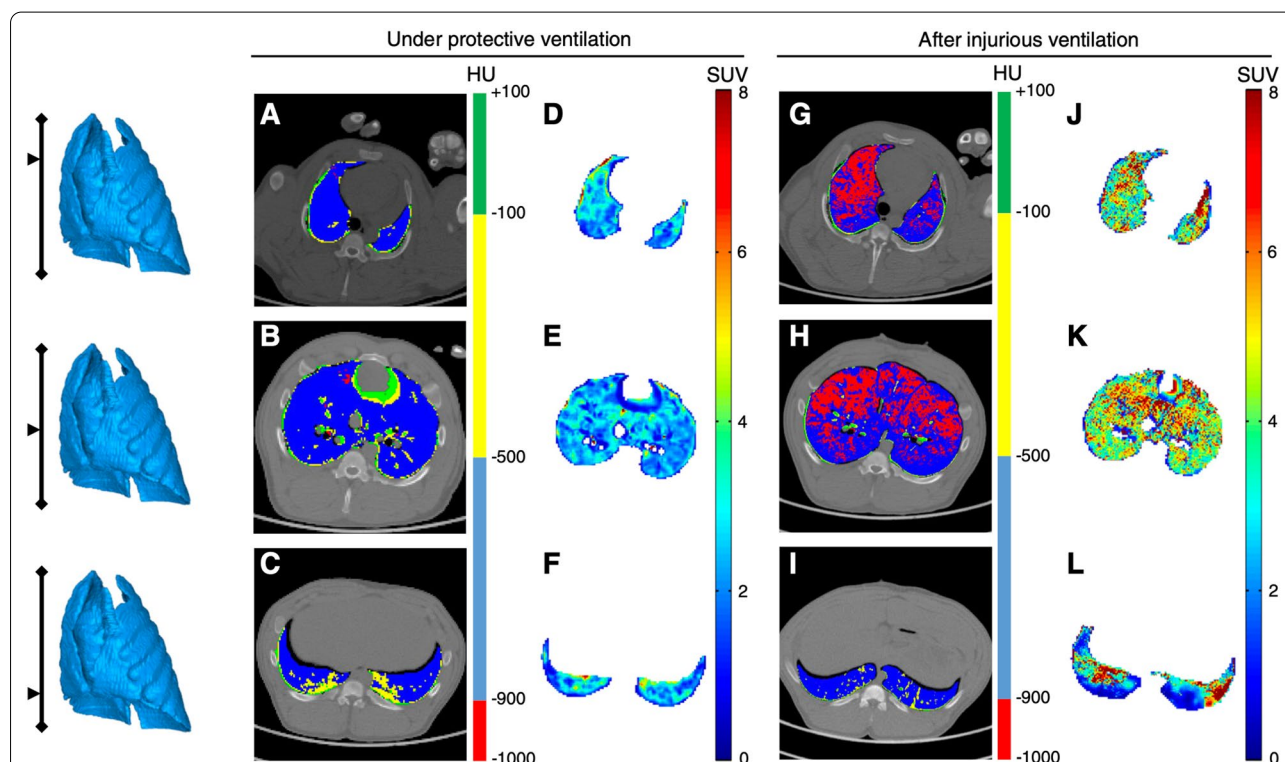
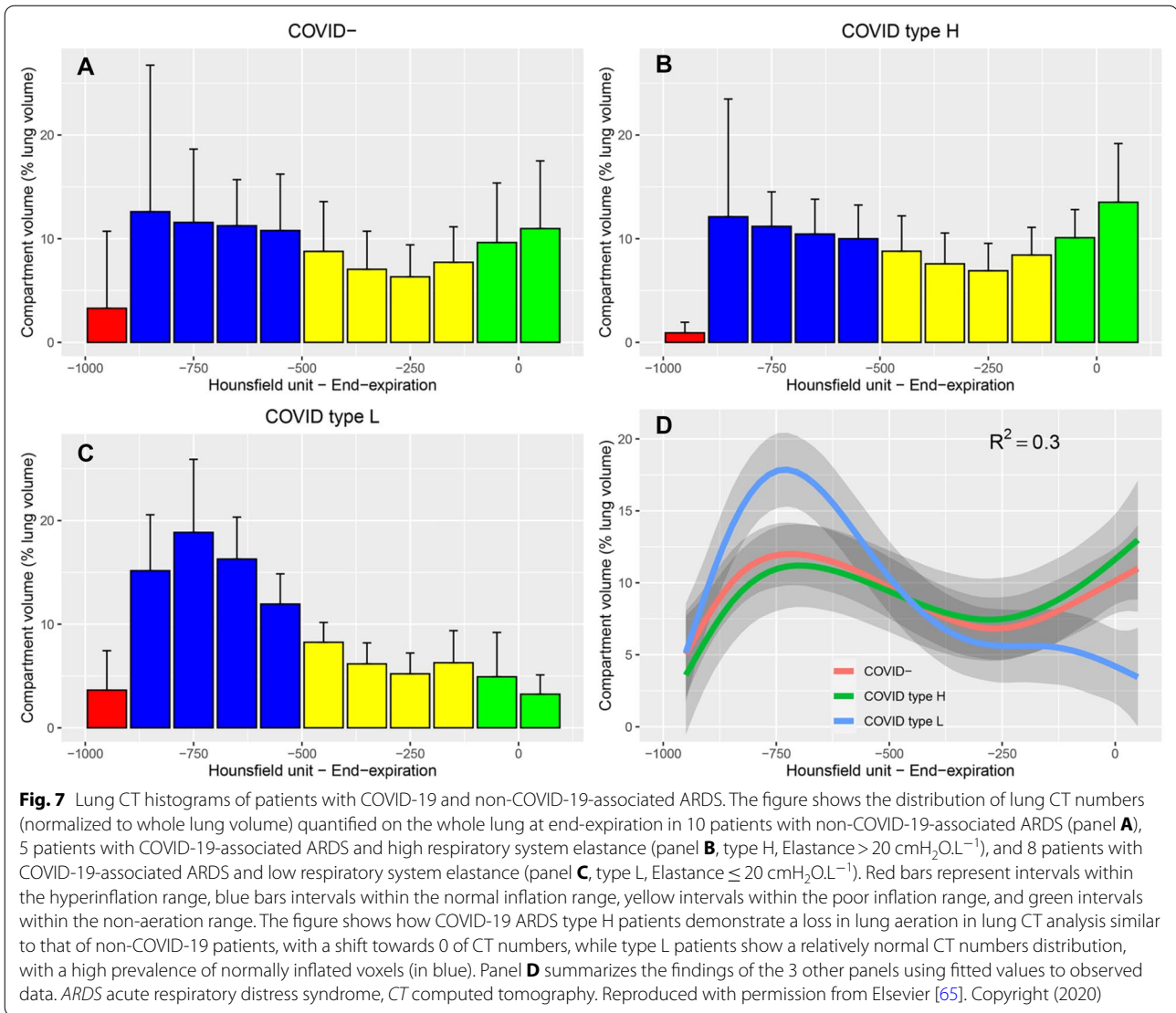


Fig. 6 Acute lung macrophage inflammation in response to high tidal volume ventilation. The figure shows the coupled PET-CT acquisitions in 3 lung slices acquired in the same animal, before and after 4 h of high tidal ventilation (targeting a transpulmonary pressure between 35 and 40 cmH_2O). PET was performed using [^{11}C](R)-PK11195, a TSPO-specific PET radiotracer that allow the non-invasive quantification of lung macrophages. CT acquisitions are performed at end-inspiration and are shown as parametric images in which the voxel's CT number is expressed based on the 4 inflation compartments (see color scale). The figure shows how the radiotracer's lung uptake (in SUV) is increased in all lung regions after injurious ventilation; this is especially true in ventral lung areas, where hyperinflation is distributed (red voxels on the end-inspiratory CT slices). CT computed tomography, HU Hounsfield unit, PET positron emission tomography, SUV standardized uptake value



the logistic and patient safety challenges that this technique imply.

What imaging taught us about COVID-19 ARDS

SARS-CoV-2-associated ARDS is easily identifiable on chest CT due to the bilateral distribution of alveolar and ground-glass opacities in the subpleural spaces, frequently associated with dependent alveolar consolidation [63]. Chiumello and colleagues showed that patients with ARDS due to coronavirus disease 2019 (COVID-19) were more hypoxemic than non-COVID-19 when matched on similar respiratory system compliance, and that venous admixture was not related to the extent of non-aerated lung volume in COVID-19 ARDS, suggesting that the clinical severity of COVID-19 ARDS was partly due to worsening

perfusion-ventilation mismatch and pulmonary vasculature impairment [64]. In another study comparing COVID-19 and non-COVID-19 ARDS, the former was associated with significantly less non-aerated lung volume on CT [65]. The authors confirmed that the lung aeration histograms of COVID-19 patients with a low elastance were significantly shifted towards low CT values, compared to non-COVID-19 ARDS or COVID-19 ARDS with low elastance (Fig. 7) [66]. More recently, Protti and colleagues showed that recruitment accounted for 24% of the whole lung tissue from PEEP 5 to 45 cmH₂O, a value significantly larger than that reported by others [20, 25].

In a study using EIT to select the best PEEP based on the collapse-overdistension compromise, Perier and colleagues showed that COVID-19 ARDS was associated

with a significantly higher selected PEEP, compared to non-COVID-19 ARDS. Secondly, the authors found that EIT did not identify differences in the response to PEEP between low elastance and high elastance COVID-19 ARDS. However, the amount of alveolar collapse was variable across COVID-19 studies, in relation to varying ventilatory management, patient morphometry (presence of obesity) and timing of EIT measurements [67]. Finally, EIT and LUS allowed the demonstration that awake prone positioning induced lung re-aeration of dorsolateral lung regions, in conjunction with changes in positive pressure levels, with potentially important effects on patient outcomes [68, 69].

Identifying complications of ARDS

Lung imaging, especially lung CT, is a key tool to help identify complications that may occur during ARDS management that may not be easily identifiable on the lung chest radiograph. Pneumothoraxes and pneumomediastinum are frequent, ranging from 10 to 20% in observational cohorts, although the incidence is decreasing since the advent of the protective ventilation era [70, 71]. Anterior pneumothoraxes are difficult to identify on anterior chest X-ray radiographs, and lung CT or LUS are useful to rapidly rule out this complication. Likewise, LUS can accurately diagnose and quantify pleural effusions which may be more difficult on chest x-ray [72]. Finally, pulmonary embolism is a difficult-to-diagnose complication with a high incidence during ARDS (between 5 and 10%), and requires CT with pulmonary angiography as part of the diagnostic work-up in worsening ARDS patients [73].

ARDS imaging as a prognostication tool

A limited number of studies have evaluated the natural radiologic history of persistent ARDS. Findings such as traction bronchiectasis, intralobular or interlobular septal thickening, ground-glass opacities or honeycombing are all associated with prolonged disease and with decreased survival in ARDS [74]. Especially, the scored extent of ground-glass opacities and honeycombing was positively correlated with fibroproliferation (assessed by procollagen III concentration in the broncho-alveolar lavage) in 192 patients with ARDS [75]. These elements of CT semiology may be evaluated using CT-based scores to follow a patient's evolution over time, and assess its mortality risk [76]. On the other hand, the persistence of consolidation opacities is not usually associated with ARDS prognosis. Of note, none of the abnormalities may help distinguish between diffuse alveolar damage and organizing pneumonia [77].

Technical aspects

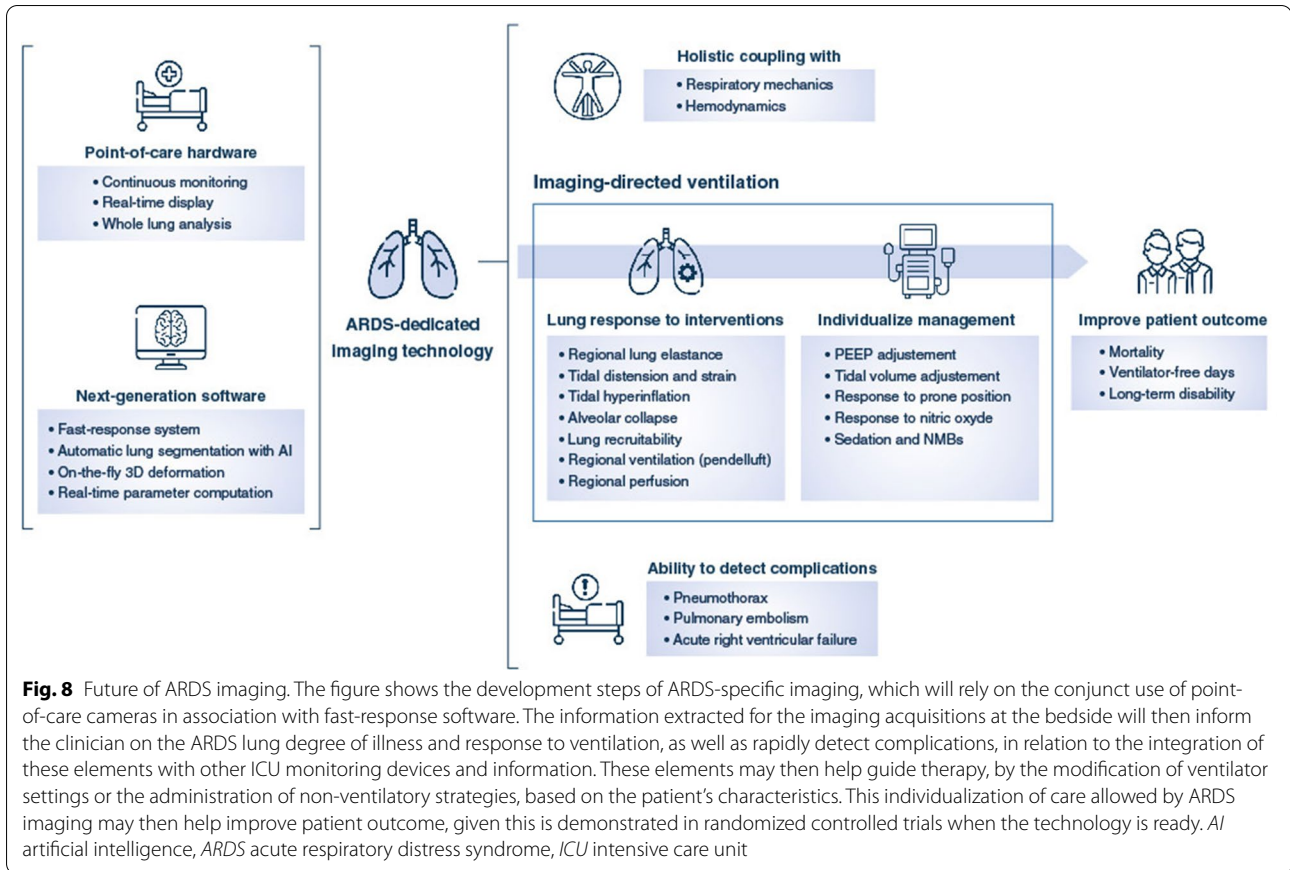
Over the last decade, numerous technological advances have allowed the acceleration of imaging research in the ARDS field. First, the implementation of low-dose chest CTs now allows the repetition of chest-centered acquisition. Second, point-of-care EIT devices allow the evaluation of the lungs' regional response to ventilatory management. The third revolution is the development of artificial intelligence and machine learning. Multiple algorithms now exist to accelerate and improve the automatic lung segmentation in CT, compared to manual segmentation, aiming to improve the identification of consolidated lung regions [78]. Artificial intelligence (AI) does not only apply to CT, but also to other lung imaging modalities such as LUS, where the software allows the identification of patterns invisible to the human eye [79]. The third and most recent development is the ability for post-processing imaging software to perform 3D deformation of lung volumes. This research tool allows the registration, deformation, and monitoring of a single voxel across multiple experimental conditions in which the regional lung volume changes and the voxel moves [39, 57].

Perspectives

The future of ARDS imaging will see the increased use of point-of-care tools that will allow whole lung analysis of anatomical, mechanistic and functional aspects of the injured lung with high granularity. These tools, augmented by AI algorithms, will improve the clinician's ability to individualize the ventilatory treatment. The first step in this process is the development of fast end-user machine-learning software programs with a real-time interpretation of image output. The second step is the choice of relevant image-derived parameters that guide ventilatory settings and impact clinical outcome. These strategies will need to be evaluated in randomized controlled clinical trials evaluating the impact of imaging-guided ventilation on patient-centered outcomes (Fig. 8). Finally, novel imaging techniques, such multi-spectral CT, might allow dynamic assessment of regional lung perfusion after contrast agent injection with high resolution, low energy and fast acquisition times.

Conclusions

The history of ARDS is closely related to that of lung imaging. Chest CT studies have led to major advances in our understanding of ARDS physiology by allowing the in vivo study of the mechanical forces that apply to the injured lungs under mechanical ventilation. Coupled with PET, morphological findings are now put in relation to functional parameters such as lung inflammation.



Point-of-care tools such as EIT or LUS, although limited in their spatial resolution, have confirmed their potential role in the assistance they bring to clinicians to improve their clinical reasoning beyond macro-respiratory mechanics, and possibly improve their ability to choose and select the best ventilation strategy. Yet, a long path remains ahead, to pursue the development of real-time, high-resolution, functional, and mechanistic imaging technologies, as an intermediate step before image-derived parameters may improve ARDS patients' outcome.

Author details

¹ Service de Médecine Intensive – Réanimation, Hôpital de la Croix Rousse, Hospices Civils de Lyon, 103 Grande Rue de la Croix Rousse, 69317 Lyon Cedex 04, France. ² Univ Lyon, INSA-Lyon, Université Claude Bernard Lyon 1, CNRS, INSERM, CREATIS UMR 5220, U1294, Villeurbanne, France. ³ Université Lyon 1 Claude Bernard, Lyon, France. ⁴ Department of Anaesthesia, Critical Care, and Pain Medicine, Beth Israel Deaconess Medical Center, Boston, MA, USA. ⁵ Harvard Medical School, Boston, MA, USA.

Author contributions

LB searched scientific databases on the subject, interpreted the results of selected articles, and drafted the manuscript. DST interpreted the results of selected articles, and made substantial revisions to the manuscript for important intellectual content. JCR interpreted the results of selected articles,

and made substantial revisions to the manuscript for important intellectual content.

Funding

None.

Declarations

Conflicts of interest

LB has declared no conflicts of interest, financial or otherwise. DST has declared funding from the National Institute for Health, Hamilton Medical, and Mindray, all outside the present work. JCR has declared funding of an experimental study by Hamilton Medical, unrelated to the present work.

Publisher's Note

Springer Nature remains neutral with regard to jurisdictional claims in published maps and institutional affiliations.

Received: 1 May 2022 Accepted: 27 June 2022

Published: 14 July 2022

References

1. The ARDS Definition Task Force (2012) Acute respiratory distress syndrome: the Berlin definition. *JAMA* 307:2526–2533
2. Brusasco C, Santori G, Tavazzi G, Via G, Robba C, Gargani L, Mojoli F, Mongodi S, Bruzzo E, Trò R, Boccacci P, Isirdi A, Forfori F, Corradi F (2022) Second-order grey-scale texture analysis of pleural ultrasound images to differentiate acute respiratory distress syndrome and cardiogenic pulmonary edema. *J Clin Monit Comput* 36:131–140

3. Wallet F, Delannoy B, Haquin A, Debord S, Leray V, Bourdin G, Bayle F, Richard JC, Bousset L, Guerin C (2013) Evaluation of recruited lung volume at inspiratory plateau pressure with PEEP using bedside digital chest X-ray in patients with acute lung injury/ARDS. *Respir Care* 58:416–423
4. Gattinoni L, Pesenti A, Bombino M, Baglioni S, Rivolta M, Rossi F, Rossi G, Fumagalli R, Marcolin R, Mascheroni D et al (1988) Relationships between lung computed tomographic density, gas exchange, and PEEP in acute respiratory failure. *Anesthesiology* 69:824–832
5. Gattinoni L, Caironi P, Pelosi P, Goodman LR (2001) What has computed tomography taught us about the acute respiratory distress syndrome? *Am J Respir Crit Care Med* 164:1701–1711
6. Goodman LR, Fumagalli R, Tagliabue P, Tagliabue M, Ferrario M, Gattinoni L, Pesenti A (1999) Adult respiratory distress syndrome due to pulmonary and extrapulmonary causes: CT, clinical, and functional correlations. *Radiology* 213:545–552
7. Gattinoni L, D'Andrea L, Pelosi P, Vitale G, Pesenti A, Fumagalli R (1993) Regional effects and mechanism of positive end-expiratory pressure in early adult respiratory distress syndrome. *JAMA* 269:2122–2127
8. Gattinoni L, Mascheroni D, Torresin A, Marcolin R, Fumagalli R, Vesconi S, Rossi GP, Rossi F, Baglioni S, Bassi F et al (1986) Morphological response to positive end expiratory pressure in acute respiratory failure. *Comput Tomogr Study Intensive Care Med* 12:137–142
9. Gattinoni L, Pelosi P, Crotti S, Valenza F (1995) Effects of positive end-expiratory pressure on regional distribution of tidal volume and recruitment in adult respiratory distress syndrome. *Am J Respir Crit Care Med* 151:1807–1814
10. Terragni PP, Rosboch G, Tealdi A, Corno E, Menaldo E, Davini O, Gandini G, Herrmann P, Mascia L, Quintel M, Slutsky AS, Gattinoni L, Ranieri VM (2007) Tidal hyperinflation during low tidal volume ventilation in acute respiratory distress syndrome. *Am J Respir Crit Care Med* 175:160–166
11. Gattinoni L, Pesenti A, Avalli L, Rossi F, Bombino M (1987) Pressure-volume curve of total respiratory system in acute respiratory failure. Computed tomographic scan study. *Am Rev Respir Dis* 136:730–736
12. Pelosi P, Goldner M, McKibben A, Adams A, Eccher G, Caironi P, Losappio S, Gattinoni L, Marini JJ (2001) Recruitment and derecruitment during acute respiratory failure: an experimental study. *Am J Respir Crit Care Med* 164:122–130
13. Cressoni M, Cadringer P, Chiurazzi C, Amini M, Gallazzi E, Marino A, Brioni M, Carlesso E, Chiumello D, Quintel M, Bugedo G, Gattinoni L (2014) Lung inhomogeneity in patients with acute respiratory distress syndrome. *Am J Respir Crit Care Med* 189:149–158
14. Cressoni M, Chiurazzi C, Gotti M, Amini M, Brioni M, Algieri I, Cammaroto A, Rovati C, Massari D, di Castiglione CB, Nikolla K, Montaruli C, Lazzarini M, Dondossola D, Colombo A, Gatti S, Valerio V, Gagliano N, Carlesso E, Gattinoni L (2015) Lung inhomogeneities and time course of ventilator-induced mechanical injuries. *Anesthesiology* 123:618–627
15. Vidal Melo MF, Layfield D, Harris RS, O'Neill K, Musch G, Richter T, Winkler T, Fischman AJ, Venegas JG (2003) Quantification of regional ventilation-perfusion ratios with PET. *J Nucl Med* 44:1982–1991
16. Schuster DP, Anderson C, Kozlowski J, Lange N (2002) Regional pulmonary perfusion in patients with acute pulmonary edema. *J Nucl Med* 43:863–870
17. Musch G, Harris RS, Vidal Melo MF, O'Neill KR, Layfield JD, Winkler T, Venegas JG (2004) Mechanism by which a sustained inflation can worsen oxygenation in acute lung injury. *Anesthesiology* 100:323–330
18. Bachmann MC, Morais C, Bugedo G, Bruhn A, Morales A, Borges JB, Costa E, Retamal J (2018) Electrical impedance tomography in acute respiratory distress syndrome. *Critical care (London, England)* 22:263
19. Richard JC, Pouzot C, Gros A, Tourevielle C, Lebars D, Lavenne F, Frerichs I, Guerin C (2009) Electrical impedance tomography compared to positron emission tomography for the measurement of regional lung ventilation: an experimental study. *Critical care (London, England)* 13:R82
20. Gattinoni L, Caironi P, Cressoni M, Chiumello D, Ranieri VM, Quintel M, Russo S, Patroniti N, Cornejo R, Bugedo G (2006) Lung recruitment in patients with the acute respiratory distress syndrome. *N Engl J Med* 354:1775–1786
21. Cressoni M, Chiumello D, Algieri I, Brioni M, Chiurazzi C, Colombo A, Colombo A, Crimella F, Guanziroli M, Tomic I, Tonetti T, Luca Vergani G, Carlesso E, Gasparovic V, Gattinoni L (2017) Opening pressures and atelectrauma in acute respiratory distress syndrome. *Intensive Care Med* 43:603–611
22. Protti A, Andreis DT, Milesi M, Iapichino GE, Monti M, Comini B, Pagni P, Melis V, Santini A, Dondossola D, Gatti S, Lombardi L, Votta E, Carlesso E, Gattinoni L (2015) Lung anatomy, energy load, and ventilator-induced lung injury. *Intensive Care Med* 3:34
23. Borges JB, Okamoto VN, Matos GF, Carames MP, Arantes PR, Barros F, Souza CE, Victorino JA, Kacmarek RM, Barbas CS, Carvalho CR, Amato MB (2006) Reversibility of lung collapse and hypoxemia in early acute respiratory distress syndrome. *Am J Respir Crit Care Med* 174:268–278
24. Ranieri VM, Eissa NT, Corbeil C, Chasse M, Braid J, Matar N, Milic-Emili J (1991) Effects of positive end-expiratory pressure on alveolar recruitment and gas exchange in patients with the adult respiratory distress syndrome. *Am Rev Respir Dis* 144:544–551
25. Protti A, Santini A, Pennati F, Chiurazzi C, Cressoni M, Ferrario M, Iapichino GE, Careno L, Lanza E, Picardo G, Caironi P, Aliverti A, Cecconi M (2022) Lung response to a higher positive end-expiratory pressure in mechanically ventilated patients with COVID-19. *Chest* 161:979–988
26. Chiumello D, Marino A, Brioni M, Menga F, Cigada I, Lazzarini M, Andrisani MC, Biondetti P, Cesana B, Gattinoni L (2013) Visual anatomical lung CT scan assessment of lung recruitability. *Intensive Care Med* 39:66–73
27. Bouhemad B, Brisson H, Le-Guen M, Arbelot C, Lu Q, Rouby JJ (2011) Bed-side ultrasound assessment of positive end-expiratory pressure-induced lung recruitment. *Am J Respir Crit Care Med* 183:341–347
28. Stefanidis K, Dimopoulos S, Tripodaki ES, Vitzialos K, Politis P, Piperopoulos P, Nanas S (2011) Lung sonography and recruitment in patients with early acute respiratory distress syndrome: a pilot study. *Critical care (London, England)* 15:R185
29. Tang KQ, Yang SL, Zhang B, Liu HX, Ye DY, Zhang HZ, Ma S (2017) Ultrasonic monitoring in the assessment of pulmonary recruitment and the best positive end-expiratory pressure. *Medicine (Baltimore)* 96:e8168
30. Victorino JA, Borges JB, Okamoto VN, Matos GF, Tucci MR, Carames MP, Tanaka H, Sipmann FS, Santos DC, Barbas CS, Carvalho CR, Amato MB (2004) Imbalances in regional lung ventilation: a validation study on electrical impedance tomography. *Am J Respir Crit Care Med* 169:791–800
31. Mauri T, Bellani G, Confalonieri A, Tagliabue P, Turella M, Coppadoro A, Citerio G, Patroniti N, Pesenti A (2013) Topographic distribution of tidal ventilation in acute respiratory distress syndrome: effects of positive end-expiratory pressure and pressure support. *Crit Care Med* 41:1664–1673
32. Spadaro S, Mauri T, Bohm SH, Scaramuzza G, Turrini C, Waldmann AD, Ragazzi R, Pesenti A, Volta CA (2018) Variation of poorly ventilated lung units (silent spaces) measured by electrical impedance tomography to dynamically assess recruitment. *Critical care (London, England)* 22:26
33. Wolf GK, Gómez-Laberge C, Rettig JS, Vargas SO, Smallwood CD, Prabhu SP, Vitali SH, Zurakowski D, Arnold JH (2013) Mechanical ventilation guided by electrical impedance tomography in experimental acute lung injury. *Crit Care Med* 41:1296–1304
34. Becher T, Buchholz V, Hassel D, Meinel T, Schadler D, Frerichs I, Weiler N (2021) Individualization of PEEP and tidal volume in ARDS patients with electrical impedance tomography: a pilot feasibility study. *Ann Intensive Care* 11:89
35. Francheineau G, Brechot N, Lebreton G, Hekimian G, Nieszkowska A, Trouillet JL, Leprince P, Chastre J, Luyt CE, Combes A, Schmidt M (2017) Bedside contribution of electrical impedance tomography to setting positive end-expiratory pressure for extracorporeal membrane oxygenation-treated patients with severe acute respiratory distress syndrome. *Am J Respir Crit Care Med* 196:447–457
36. He H, Chi Y, Yang Y, Yuan S, Long Y, Zhao P, Frerichs I, Fu F, Möller K, Zhao Z (2021) Early individualized positive end-expiratory pressure guided by electrical impedance tomography in acute respiratory distress syndrome: a randomized controlled clinical trial. *Critical care (London, England)* 25:230
37. Dreyfuss D, Saumon G (1993) Role of tidal volume, FRC, and end-inspiratory volume in the development of pulmonary edema following mechanical ventilation. *Am Rev Respir Dis* 148:1194–1203
38. Protti A, Andreis DT, Monti M, Santini A, Sparacino CC, Langer T, Votta E, Gatti S, Lombardi L, Leopardi O, Masson S, Cressoni M, Gattinoni L (2013) Lung stress and strain during mechanical ventilation: any difference between statics and dynamics? *Crit Care Med* 41:1046–1055
39. Motta-Ribeiro GC, Hashimoto S, Winkler T, Baron RM, Grogg K, Paula L, Santos A, Zeng C, Hibbert K, Harris RS, Bajwa E, Vidal Melo MF (2018)

- Deterioration of regional lung strain and inflammation during early lung injury. *Am J Respir Crit Care Med* 198:891–902
40. Bitker L, Costes N, Le Bars D, Lavenne F, Orkisz M, Hernandez Hoyos M, Benzerdjeb N, Devouassoux M, Richard JC (2019) Noninvasive quantification of macrophagic lung recruitment during experimental ventilation-induced lung injury. *J Appl Physiol* 127:546–558
 41. Reske AW, Busse H, Amato MB, Jaekel M, Kahn T, Schwarzkopf P, Schreiter D, Gottschaldt U, Seiwerts M (2008) Image reconstruction affects computer tomographic assessment of lung hyperinflation. *Intensive Care Med* 34:2044–2053
 42. Beda A, Carvalho AR, Carvalho NC, Hammermuller S, Amato MB, Muders T, Gittel C, Kavanagh K, Wrigge H, Reske AW (2017) Mapping regional differences of local pressure-volume curves with electrical impedance tomography. *Crit Care Med* 45:679–686
 43. Meier T, Luepschen H, Karsten J, Leibbecke T, Grossherr M, Gehring H, Leonhardt S (2008) Assessment of regional lung recruitment and derecruitment during a PEEP trial based on electrical impedance tomography. *Intensive Care Med* 34:543–550
 44. Yoshida T, Torsani V, Gomes S, De Santis RR, Beraldo MA, Costa EL, Tucci MR, Zin WA, Kavanagh BP, Amato MB (2013) Spontaneous effort causes occult pendelluft during mechanical ventilation. *Am J Respir Crit Care Med* 188:1420–1427
 45. Muders T, Luepschen H, Zinserling J, Greschus S, Fimmers R, Guenther U, Buchwald M, Grigutsch D, Leonhardt S, Putensen C, Wrigge H (2012) Tidal recruitment assessed by electrical impedance tomography and computed tomography in a porcine model of lung injury*. *Crit Care Med* 40:903–911
 46. Gattinoni L, Pelosi P, Vitale G, Pesenti A, D'Andrea L, Mascheroni D (1991) Body position changes redistribute lung computed-tomographic density in patients with acute respiratory failure. *Anesthesiology* 74:15–23
 47. Cornejo RA, Diaz JC, Tobar EA, Bruhn AR, Ramos CA, Gonzalez RA, Repetto CA, Romero CM, Galvez LR, Llanos O, Arellano DH, Neira WR, Diaz GA, Zamorano AJ, Pereira GL (2013) Effects of prone positioning on lung protection in patients with acute respiratory distress syndrome. *Am J Respir Crit Care Med* 188:440–448
 48. Perchiazzi G, Rylander C, Vena A, Derosa S, Polieri D, Fiore T, Giuliani R, Hedenstierna G (1985) (2011) Lung regional stress and strain as a function of posture and ventilatory mode. *J Appl Physiol* 110:1374–1383
 49. Richard JC, Le Bars D, Costes N, Bregeon F, Tourvieille C, Lavenne F, Janier M, Gimenez G, Guerin C (2006) Alveolar recruitment assessed by positron emission tomography during experimental acute lung injury. *Intensive Care Med* 32:1889–1894
 50. Richard JC, Bregeon F, Costes N, Bars DL, Tourvieille C, Lavenne F, Janier M, Bourdin G, Gimenez G, Guerin C (2008) Effects of prone position and positive end-expiratory pressure on lung perfusion and ventilation. *Crit Care Med* 36:2373–2380
 51. Richard JC, Janier M, Lavenne F, Berthier V, Lebars D, Annat G, Decailliot F, Guerin C (2002) Effect of position, nitric oxide, and almitrine on lung perfusion in a porcine model of acute lung injury. *J Appl Physiol* (1985) 93:2181–2191
 52. Richter T, Bellani G, Scott Harris R, Vidal Melo MF, Winkler T, Venegas JG, Musch G (2005) Effect of prone position on regional shunt, aeration, and perfusion in experimental acute lung injury. *Am J Respir Crit Care Med* 172:480–487
 53. Schroeder T, Vidal Melo MF, Musch G, Harris RS, Venegas JG, Winkler T (2008) Modeling pulmonary kinetics of 2-deoxy-2-[18F]fluoro-D-glucose during acute lung injury. *Acad Radiol* 15:763–775
 54. Saha D, Takahashi K, de Prost N, Winkler T, Pinilla-Vera M, Baron RM, Vidal Melo MF (2013) Micro-autoradiographic assessment of cell types contributing to 2-deoxy-2-[18F]fluoro-D-glucose uptake during ventilator-induced and endotoxemic lung injury. *Mol Imaging Biol* 15:19–27
 55. Bellani G, Guerra L, Musch G, Zanella A, Patroniti N, Mauri T, Messa C, Pesenti A (2011) Lung regional metabolic activity and gas volume changes induced by tidal ventilation in patients with acute lung injury. *Am J Respir Crit Care Med* 183:1193–1199
 56. Musch G, Venegas JG, Bellani G, Winkler T, Schroeder T, Petersen B, Harris RS, Melo MF (2007) Regional gas exchange and cellular metabolic activity in ventilator-induced lung injury. *Anesthesiology* 106:723–735
 57. Retamal J, Hurtado D, Villarroel N, Bruhn A, Buggedo G, Amato MBP, Costa ELV, Hedenstierna G, Larsson A, Borges JB (2018) Does regional lung strain correlate with regional inflammation in acute respiratory distress syndrome during nonprotective ventilation? An experimental porcine study. *Crit Care Med* 46:e591–e599
 58. Guldner A, Braune A, Ball L, Silva PL, Samary C, Inorsi A, Huhle R, Rentzsch I, Becker C, Oehme L, Andreeff M, Vidal Melo MF, Winkler T, Pelosi P, Rocco PR, Kotzerke J, Gama de Abreu M (2016) Comparative effects of volutrauma and atelectrauma on lung inflammation in experimental acute respiratory distress syndrome. *Crit Care Med* 44:e854–865
 59. Wakabayashi K, Wilson MR, Tatham KC, O'Dea KP, Takata M (2014) Volutrauma, but not atelectrauma, induces systemic cytokine production by lung-marginated monocytes. *Crit Care Med* 42:e49–57
 60. Hatori A, Yui J, Yamasaki T, Xie L, Kumata K, Fujinaga M, Yoshida Y, Ogawa M, Nengaki N, Kawamura K, Fukumura T, Zhang MR (2012) PET imaging of lung inflammation with [18F]FEDAC, a radioligand for translocator protein (18 kDa). *PLoS ONE* 7:e45065
 61. Lambrou T, Groves AM, Erlandsson K, Screation N, Endozo R, Win T, Porter JC, Hutton BF (2011) The importance of correction for tissue fraction effects in lung PET: preliminary findings. *Eur J Nucl Med Mol Imaging* 38:2238–2246
 62. Bitker L, Dhelft F, Lancelot S, Le Bars D, Costes N, Benzerdjeb N, Orkisz M, Richard JC (2022) Non-invasive quantification of acute macrophagic lung inflammation with [(11)C](R)-PK11195 using a three-tissue compartment kinetic model in experimental acute respiratory distress syndrome. *Eur J Nucl Med Mol Imaging* 49(7):2122–2136
 63. Yang H, Lan Y, Yao X, Lin S, Xie B (2020) The chest CT features of coronavirus disease 2019 (COVID-19) in China: a meta-analysis of 19 retrospective studies. *Virol J* 17:159
 64. Chiumello D, Busana M, Coppola S, Romitti F, Formenti P, Bonifazi M, Pozzi T, Palumbo MM, Cressoni M, Herrmann P, Meissner K, Quintel M, Camporota L, Marini JJ, Gattinoni L (2020) Physiological and quantitative CT-scan characterization of COVID-19 and typical ARDS: a matched cohort study. *Intensive Care Med* 46:2187–2196
 65. Chauvelot L, Bitker L, Dhelft F, Mezidi M, Orkisz M, Davila Serrano E, Penarubia L, Yonis H, Chabert P, Folliet L, David G, Provoost J, Lecam P, Bousset L, Richard JC (2020) Quantitative-analysis of computed tomography in COVID-19 and non COVID-19 ARDS patients: a case-control study. *J Crit Care* 60:169–176
 66. Gattinoni L, Chiumello D, Caironi P, Busana M, Romitti F, Brazzi L, Camporota L (2020) COVID-19 pneumonia: different respiratory treatments for different phenotypes? *Intensive Care Med* 46:1099–1102
 67. van der Zee P, Somhorst P, Endeman H, Gommers D (2020) Electrical impedance tomography for positive end-expiratory pressure titration in COVID-19-related acute respiratory distress syndrome. *Am J Respir Crit Care Med* 202:280–284
 68. Rauseo M, Mirabella L, Laforgia D, Lamanna A, Vetusch P, Soriano E, Ugliola D, Casiello E, Tullo L, Cinnella G (2021) A pilot study on electrical impedance tomography during CPAP trial in Patients With Severe Acute Respiratory Syndrome Coronavirus 2 Pneumonia: The Bright Side Of Non-Invasive Ventilation. *Front Physiol* 12:728243
 69. Musso G, Taliano C, Molinaro F, Fonti C, Veliaj D, Torti D, Paschetta E, Castagna E, Carbone G, Laudari L, Aseglio C, Zocca E, Chioni S, Giannone LC, Arabia F, Deiana C, Benato FM, Druetta M, Campagnola G, Borsari M, Mucci M, Rubatto T, Peyronel M, Tirabassi G (2022) Early prolonged prone position in noninvasively ventilated patients with SARS-CoV-2-related moderate-to-severe hypoxemic respiratory failure: clinical outcomes and mechanisms for treatment response in the PRO-NIV study. *Critical care (London, England)* 26:118
 70. Terzi E, Zarogoulidis K, Kougioumtzi I, Dryllis G, Kioumis I, Pitsiou G, Machairiotis N, Katsikogiannis N, Lampaki S, Papaiwannou A, Tsiouda T, Madesis A, Karaiskos T, Zaric B, Branislav P, Zarogoulidis P (2014) Acute respiratory distress syndrome and pneumothorax. *J Thorac Dis* 6:S435–442
 71. Network TARDS (2000) Ventilation with lower tidal volumes as compared with traditional tidal volumes for acute lung injury and the acute respiratory distress syndrome. *N Engl J Med* 342:1301–1308
 72. Lichtenstein D, Goldstein I, Mourgeon E, Cluzel P, Grenier P, Rouby JJ (2004) Comparative diagnostic performances of auscultation, chest radiography, and lung ultrasonography in acute respiratory distress syndrome. *Anesthesiology* 100:9–15
 73. de Roubin V, Reynaud F, Coudroy R, Rodriguez M, Monseau G, Joly F, Bardin J, Boissier F, Chatellier D, Veinstein A, Robert R, Frat JP, Thille AW (2021) High risk of pulmonary embolism in acute respiratory distress syndrome

- related to COVID-19: an observational controlled-cohort study. *Ann Transl Med* 9:630
74. Ichikado K, Suga M, Muranaka H, Gushima Y, Miyakawa H, Tsubamoto M, Johkoh T, Hirata N, Yoshinaga T, Kinoshita Y, Yamashita Y, Sasaki Y (2006) Prediction of prognosis for acute respiratory distress syndrome with thin-section CT: validation in 44 cases. *Radiology* 238:321–329
 75. Hamon A, Scemama U, Bourenne J, Daviet F, Coiffard B, Persico N, Adda M, Guervilly C, Hraiech S, Chaumoitre K, Roch A, Papazian L, Forel JM (2019) Chest CT scan and alveolar procollagen III to predict lung fibroproliferation in acute respiratory distress syndrome. *Ann Intensive Care* 9:42
 76. Rouby JJ, Puybasset L, Cluzel P, Richecoeur J, Lu Q, Grenier P (2000) Regional distribution of gas and tissue in acute respiratory distress syndrome. II. Physiological correlations and definition of an ARDS Severity Score. *CT Scan ARDS Study Group. Intensive Care Med* 26:1046–1056
 77. Chung JH, Kradin RL, Greene RE, Shepard JA, Digumarthy SR (2011) CT predictors of mortality in pathology confirmed ARDS. *Eur Radiol* 21:730–737
 78. Herrmann P, Busana M, Cressoni M, Lotz J, Moerer O, Saager L, Meissner K, Quintel M, Gattinoni L (2021) Using artificial intelligence for automatic segmentation of CT lung images in acute respiratory distress syndrome. *Front Physiol* 12:676118
 79. Mantuani D, Nagdev A, Stone M (2012) Three-view bedside ultrasound for the differentiation of acute respiratory distress syndrome from cardiogenic pulmonary edema. *Am J Emerg Med* 30:1324.e1321-1324